

## Article

# Accessing the Heat Exposure Risk in Beijing–Tianjin–Hebei Region Based on Heat Island Footprint Analysis

Xuecheng Fu , Lei Yao \* and Shuo Sun

College of Geography and Environment, Shandong Normal University, Jinan 250300, China; ferwinjohn@163.com (X.F.); sdu\_ss@163.com (S.S.)

\* Correspondence: alex\_yaolei@126.com

**Abstract:** The urbanization process leads to the enhancement of the urban heat island (UHI) effect, and the high temperature brought by it exacerbates the risk of heat exposure and seriously endangers human health. Analyzing the spatiotemporal characteristics and levels of heat exposure risk is important for formulating heat risk prevention and control measures. Therefore, this study analyzes the spatiotemporal characteristics of heat exposure risk based on the UHI footprint (FP) and explores the relationship between it and urbanization factors in the Beijing–Tianjin–Hebei (BTH) region from 2000 to 2020, and obtains the following conclusions: (1) The BTH region suffers from severe UHI problems, with FP ranging from 6.05 km (Chengde) to 32.51 km (Beijing), and the majority of cities show significant trends of FP increase. (2) With the increase in FP, massive populations are exposed within the heat risk areas, with the average annual population at risk across cities ranging from 269,826 (Chengde) to 166,020,390 (Beijing), with a predominance of people exposed to high risk (more than 65% of the total) and generally showing increasing trends. (3) The population at risk of heat exposure is significantly correlated with urbanization factors, indicating that urbanization is an important reason for the increase in the risk population and the enhancement of the risk level. These results suggest that with the continuous urbanization process, the heat exposure risk problem faced by cities in the BTH region will persist and gradually worsen, which must be paid attention to and effective mitigation measures must be taken.

**Keywords:** heat island footprint; heat exposure risk; single exponential decay model; urbanization; Beijing–Tianjin–Hebei



**Citation:** Fu, X.; Yao, L.; Sun, S. Accessing the Heat Exposure Risk in Beijing–Tianjin–Hebei Region Based on Heat Island Footprint Analysis. *Atmosphere* **2022**, *13*, 739. <https://doi.org/10.3390/atmos13050739>

Academic Editors: Mikhail Lokoshchenko, Lyubov Alekseeva and Kishor Zingre

Received: 26 February 2022

Accepted: 2 May 2022

Published: 5 May 2022

**Publisher's Note:** MDPI stays neutral with regard to jurisdictional claims in published maps and institutional affiliations.



**Copyright:** © 2022 by the authors. Licensee MDPI, Basel, Switzerland. This article is an open access article distributed under the terms and conditions of the Creative Commons Attribution (CC BY) license (<https://creativecommons.org/licenses/by/4.0/>).

## 1. Introduction

According to the World Cities Report 2020 published by UN-Habitat, the proportion of the global urban population will exceed 60% by 2030, and land for urban construction is expanding at twice the rate of population growth, which has a great impact on the surface landscape and local climate [1–4]. In the process of urbanization, the natural surface is gradually converted to an artificial surface, which causes a decrease in latent heat flux and an increase in sensible heat flux in urban areas, making the temperature in urban areas significantly higher than that in the surrounding countryside, resulting in the urban heat island (UHI) effect [5]. The UHI effect not only adversely affects urban ecological safety and sustainable development, such as increasing energy consumption and deteriorating atmospheric environment [6–8], it also harms the health of urban residents, such as increasing the morbidity and mortality of urban residents from heat stress diseases [9–11], which is expected to increase the number of heat-related deaths by more than 90,000 worldwide by 2030 [12]. The relatively hot environment caused by the UHI effect can also affect normal urban production activities and increase the occupational risk of the associated heat-exposed population [13]. Currently, more than 1 billion workers remain exposed to hot weather and are susceptible to heat stress risk stimulation that can have a cumulative negative impact on their productive activities [14–16]. Therefore, it is necessary to accurately analyze and

grasp the characteristic patterns of the UHI effect and the potential heat exposure risk of its associated population, which will provide a scientific basis for scientific regulation and mitigation of urban thermal environmental risks.

Urban heat exposure risk assessment, often defined as the degree of overlap between urban population and urban heat risk or the size of the urban population affected by heat risk, can effectively integrate urban environmental issues with socio-demographic characteristics, and is of great practical importance to fully understand, effectively respond to, and actively prevent the hazards posed by the UHI effect [17,18]. The risk of heat exposure depends greatly on the impact extent of the UHI effect and the spatial distribution characteristics of the urban population, and therefore quantifying the spatial pattern characteristics of the UHI effect is the basis and prerequisite for assessing the risk of heat exposure [19]. In previous heat exposure risk studies, scholars usually conducted risk assessments based on existing geographic units (e.g., administrative divisions or urban built-up area boundaries) as the spatially constrained boundaries of the UHI effect [20,21]. However, due to the complex heat exchange between urban and rural areas, the UHI effect has obvious “spatial spillover” characteristics, and its actual impact extent often exceeds the boundary of urban built-up areas, and is not consistent with its administrative boundaries [22]. Therefore, existing assessment methods based on geographic units do not adequately and truly reflect the real characteristics of the heat exposure risk of a specific city. For this purpose, the urban heat island footprint (FP) is introduced in this study as a spatially constrained extent for assessing heat exposure risk. FP is an assessment index to characterize the impact extent of UHI extracted based on the real urban-rural land surface temperature gradient characteristics [23]. With the development of related research, various FP calculation models such as the Gaussian model and nonlinear decay model have been proposed one after another, and have been widely used in the research of spatial characteristics representation of the UHI effect [24–26]. Therefore, the FP-based research method is able to fully grasp the impact range of the UHI effect in a specific city and effectively enhance the comprehensiveness and accuracy of heat exposure risk assessment, providing scientific support for urban thermal environment management and regulation.

In this study, 13 cities in the Beijing–Tianjin–Hebei region are selected as typical cases for heat exposure risk research, and MODIS land surface temperature data, World POP population data, and socio-economic panel data are used to grasp the characteristics of surface thermal environment, population distribution, and urbanization development status in the study area respectively. Based on this, the specific objectives of this study are as follows: (1) to construct a single exponential decay model to try to extract the FP characteristics of each city in the study area; (2) to assess the status of heat exposure risk for each city under the influence of UHI; and (3) to grasp the association characteristics between urban heat exposure risk and urbanization factors.

## 2. Materials and Methods

### 2.1. Studied Region

The Beijing–Tianjin–Hebei (BTH) region is located in North China ( $113^{\circ}27' E \sim 119^{\circ}19' E$ ,  $36^{\circ}05' N \sim 42^{\circ}40' N$ ), with an area of about 218,000 km<sup>2</sup> and a warm temperate continental monsoon climate. The BTH urban agglomeration, one of the three major urban agglomerations in China, is located in this region and contains two municipalities, Beijing and Tianjin, as well as 11 prefecture-level cities under the jurisdiction of Hebei Province (Figure 1). Since the Reform and Opening Up, the region has experienced rapid socio-economic development and has become one of the most dynamic regions for urban development in China, with the population urbanization rate rising from 58.5% in 2000 to 77.42% in 2020, urban construction land increasing from 1988 km<sup>2</sup> to 3379 km<sup>2</sup>, an increase of about 1.7 times, and the Gross Domestic Product (GDP) also increasing from 947.23 billion in 2000 to 8639.32 billion in 2020, an increase of about 9.1 times [27]. However, the highly concentrated population and rapidly expanding cities have also profoundly changed the local surface thermal environment. Previous studies have shown that the UHI intensity

in the BTH region is increasing significantly at a rate of  $0.10\text{ }^{\circ}\text{C}/\text{year}$ , and the spatial extent is rapidly increasing, expanding and connecting, gradually forming a large UHI agglomeration area [28]. The continuous deterioration of the urban thermal environment has negatively affected the habitat and the health of residents in the region, thus triggering widespread concern among urban managers and related scholars [29].

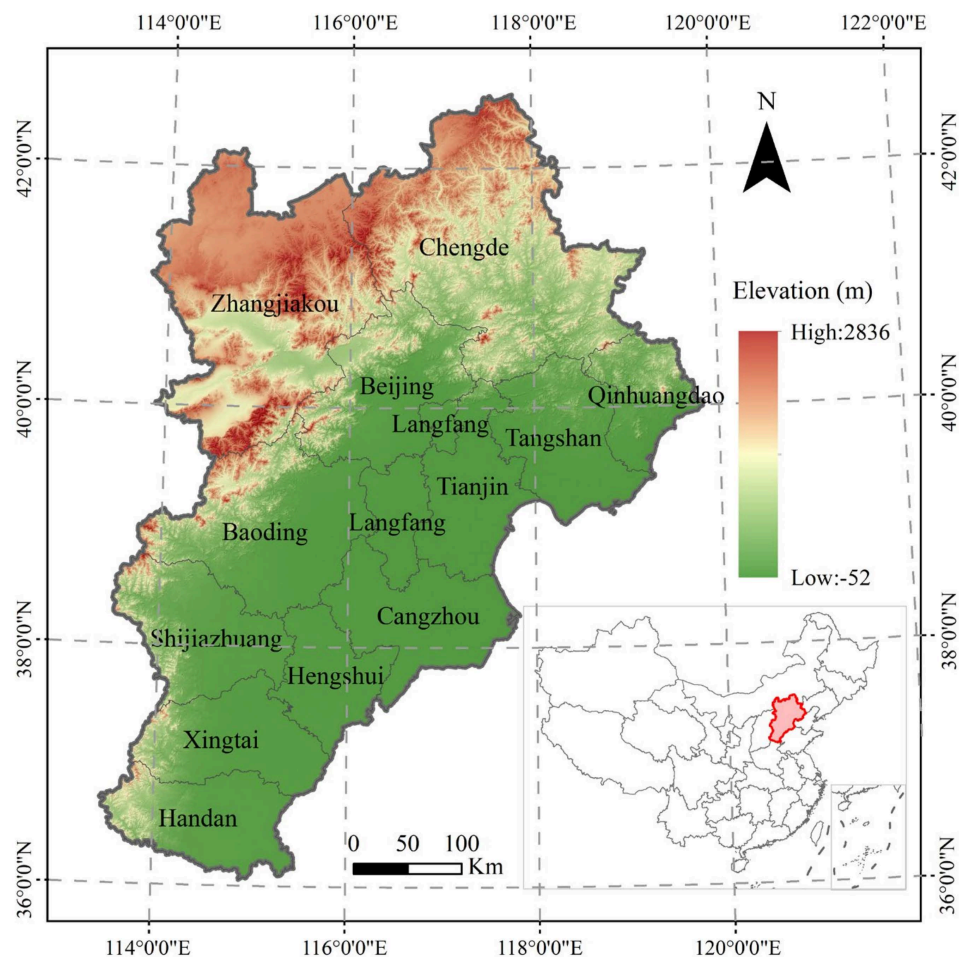


**Figure 1.** Elevation, location, and distribution of cities in the Beijing–Tianjin–Hebei (BTH) region.

## 2.2. Data sources

### 2.2.1. Land Surface Temperature Data

In this study, we use the 8-day synthetic daytime land surface temperature (LST) product (MOD11A2, <https://ladsweb.modaps.eosdis.nasa.gov/>, accessed on 20 September 2021) acquired by the Moderate-Resolution Imaging Spectroradiometer (MODIS) during the summer (June–August) from 2000 to 2020. The product has a spatial resolution of 1 km and is obtained based on surface thermal radiation estimated by a split-window algorithm, with an accuracy better than 1 K which can effectively reflect the LST conditions in cities and their surrounding areas [30]. The MODIS Reprojection Tool is used to pre-process the LST data, including projection, mosaic, and cropping, and the initial 8-day synthetic data are averaged to the summer LST data using the ArcGIS cell statistics function.

### 2.2.2. Population Data

The population data used in this study are obtained from the raster data on the distribution of the world's population (2000–2020) provided by the WorldPop project (<http://www.worldpop.org.uk/>, accessed on 7 October 2021), with a spatial resolution of 1 km. The data combines data from multiple sources such as census databases, land cover data, night-time light intensity and habitat, and is spatially processed through a

random forest model to estimate the precise population size of the area. Due to the high accuracy and spatial resolution of the data, it is widely used in population-based surveys and research [31,32].

### 2.2.3. Other Data

Other data used in this paper include land cover data, digital elevation model (DEM) data and GDP data for each city, which are used for the extraction of urban built-up areas, and the removal of abnormal pixels and the measurement of urbanization level, respectively. Land cover data are derived from annual landcover data provided by the European Space Agency (<https://www.esa-landcover-cci.org/>, accessed on 15 October 2021) with a spatial resolution of 300 m; DEM is from SRTM terrain product with a spatial resolution of 30 m. GDP data are derived from China City Statistical Yearbooks of various cities [33].

## 2.3. Methodology

### 2.3.1. Heat Island Footprint Modelling Extraction

The prerequisite for FP extraction lies in quantifying the gradient variation characteristics of urban-rural LST. When the UHI effect is significant, the temperature ( $T$ ) decreases gradually from the urban center to the peripheral rural areas, so the establishment of multiple buffers from the urban center outwards is an effective method to quantify the  $T$  gradient difference ( $\Delta T$ ) between urban and rural areas [23]. (1) Define the urban center. Based on the land cover data, the  $1 \times 1$  km moving window method is used to identify and extract the kilometer grid of each city with a proportion of built-up land greater than 50%, and further extract the built-up area range of each city through cluster analysis, and extract the center of gravity as the urban center [34]; (2) Establish multiple buffers. Based on the extracted urban centers, the improved equal-area method is adopted to construct 30 buffers, and the area of each buffer is consistent with the area of the built-up area of the city [35]. Please note that the study excludes the pixels of the water body as well as  $\pm 50$  m gaps in the average elevation of the urban area due to the anomalous effects of water bodies and excessive elevation on LST (Figure 2a) [36,37].

To quantify  $\Delta T$ , a reference rural  $T$  is first defined. We use the average  $T$  of the outermost three buffers as reference rural  $T$  and calculate  $\Delta T$  separately for the urban area and adjacent buffers in each city (Equation (1)), which can help to avoid potential outlier bias caused by the use of a single buffer [38].

$$\Delta T = T_b - T_{ref} \quad (1)$$

$T_b$  and  $T_{ref}$  represent the LST in each buffer and rural reference area respectively. Buffers with  $\Delta T$  greater than  $0^\circ\text{C}$  are considered to have the UHI effect, and a single exponential decay model is subsequently built to examine urban-rural  $\Delta T$  trends in each city (Equation (2)) and to extract UHI influence extent thresholds.

$$\Delta T = y_0 + A_1 \exp(-x/t_1) \quad (2)$$

where  $y_0$  is the offset,  $A_1$  is the maximum difference of  $T$ ,  $x$  is the distance from the city center and  $t_1$  is the decay rate. In this study, the slope of the fitted curve ( $S$ ) equaling  $-0.1$  is selected as the threshold value to segment the  $\Delta T$  change curve, and the buffer area within the threshold value is used as FP (Figure 2b).

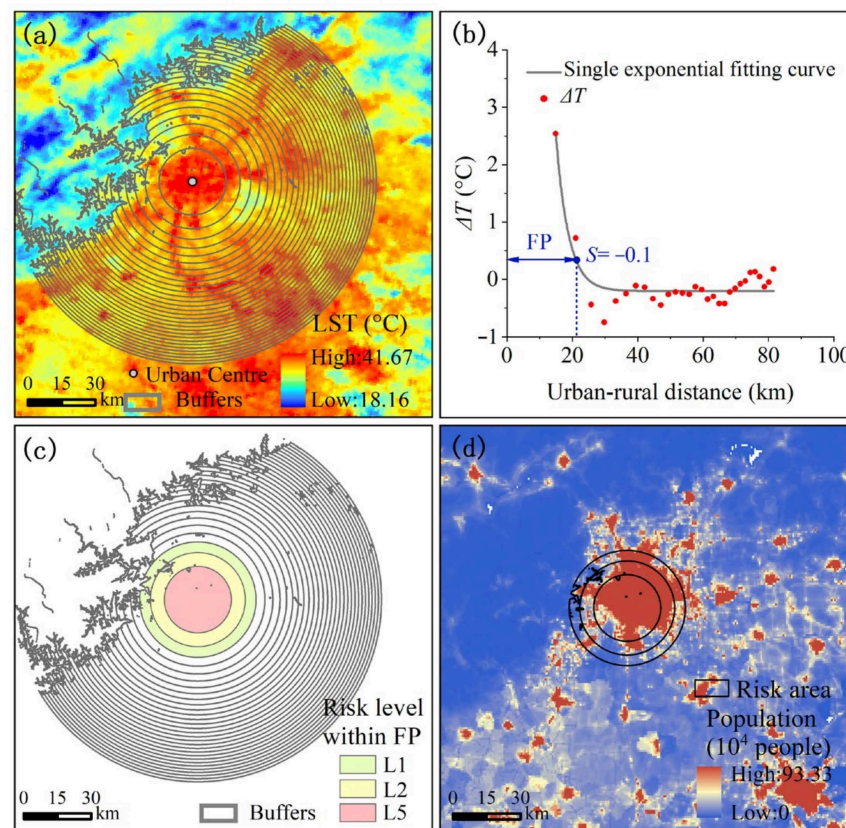


**Figure 2.** The schematic diagram of urban heat exposure risk analysis based on the footprint (FP) (taking Beijing in 2000 as an example). (a) Extraction of urban center and construction of buffer zones (LST represents land surface temperature); (b) examination of LST difference ( $\Delta T$ ) trend and extraction of FP based on Single Exponential Decay model ( $S$  represents the slope of the fitted curve); (c) classification of heat exposure risk based on  $\Delta T$ ; (d) identification of at-risk populations based on overlay analysis of risk areas and population distribution.

### 2.3.2. Heat Exposure Risk Assessment

Firstly, the mean standard deviation classification method is applied to classify the buffers within the FP of each city in the study area from 2000 to 2020 and to identify different urban heat risk class areas as a basis for measuring heat exposure risk (Table 1, Figure 2c) [39]. Subsequently, the spatial overlay analysis of the heat exposure risk class areas and the population data of the corresponding years is carried out to obtain the population characteristics of the multiple levels of heat exposure risk areas in each city of the study area (Figure 2d).

**Table 1.** Heat exposure risk classification criteria.

Risk level	Level Description	Range of Values <sup>1</sup>
L1	low heat exposure risk	$0 < \Delta T < \mu - 1/2\sigma$
L2	Medium-low heat exposure risk	$\mu - 1/2\sigma < \Delta T < \mu + 1/2\sigma$
L3	Medium heat exposure risk	$\mu + 1/2\sigma < \Delta T < \mu + 3/2\sigma$
L4	Medium-high heat exposure risk	$\mu + 3/2\sigma < \Delta T < \mu + 5/2\sigma$
L5	High heat exposure risk	$\mu + 5/2\sigma < \Delta T$

<sup>1</sup>  $\mu$  is the average value of each buffer  $\Delta T$  and  $\sigma$  is the standard deviation.

### 2.3.3. Analysis of the Association between Heat Exposure Risk and the Urbanization Process

According to previous studies, population density (PD), GDP and built-up area (BUA) can be used as key indicators for measuring the degree of urbanization, characterizing the process of population urbanization, economic urbanization and land urbanization respectively [40,41]. Therefore, these three urbanization factors are chosen in this study to explore the relationship between the urbanization process and the urban heat exposure risk. Curve fitting analyses are conducted with the population at risk of heat exposure as the dependent variable and the urbanization factors as the independent variables. The optimal characteristic relationship curve is then selected to represent the relationship between urbanization factors and urban heat exposure risk based on the coefficient of determination ( $R^2$ ) and significance test ( $p < 0.05$ ).

## 3. Results

### 3.1. Heat Island Footprint Characteristics of Cities in the Beijing–Tianjin–Hebei Region

According to the ANOVA analysis of the FP characteristics in the cities during the period 2000–2020 (Figure 3), Beijing presents the largest FP with an annual mean of 32.51 km; followed by Tianjin, Tangshan and Shijiazhuang, with their respective means of 17.84, 17.53 and 17.38 km; followed by Qinhuangdao, Handan and Baoding, with their respective means of 13.65, 13.31 and 13.26 km. The remaining cities, with relatively small FP, are Langfang (9.82 km), Hengshui (9.42 km), Xingtai (9.03 km), Zhangjiakou (8.81 km), Cangzhou (7.99 km) and Chengde (6.05 km).

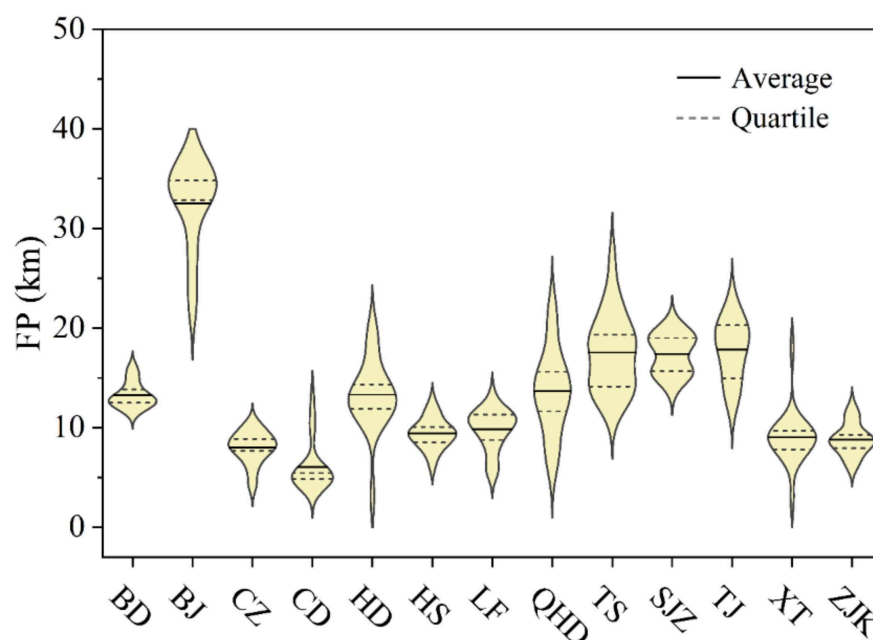


**Figure 3.** Differences in FP among cities in the BTH region from 2000 to 2020 (based on ANOVA analysis). BD: Baoding, BJ: Beijing, CZ: Cangzhou, CD: Chengde, HD: Handan, HS: Hengshui, LF: Langfang, QHD: Qinhuangdao, TS: Tangshan, SJZ: Shijiazhuang, TJ: Tianjin, XT: Xingtai, and ZJK: Zhangjiakou.

In addition, most cities in the BTH region show significant increasing trends in FP between 2000 and 2020 ( $p < 0.01$ ), as shown in Figure 4. Among the 13 cities in the BTH region, 10 cities show linear increasing trends of FP, and eight cities show significant increasing trends ( $p < 0.01$ ), with the fastest increase in FP being in Tangshan, with an annual average growth of 0.56 km, followed by Xingtai, Zhangjiakou, Beijing, Langfang, Shijiazhuang and Cangzhou, with an average annual growth rate of more than 0.20 km/year. In contrast,

relatively few cities show decreasing trends of FP, being only three cities, Qinhuangdao, Tianjin and Handan, but none of their trends is significant.

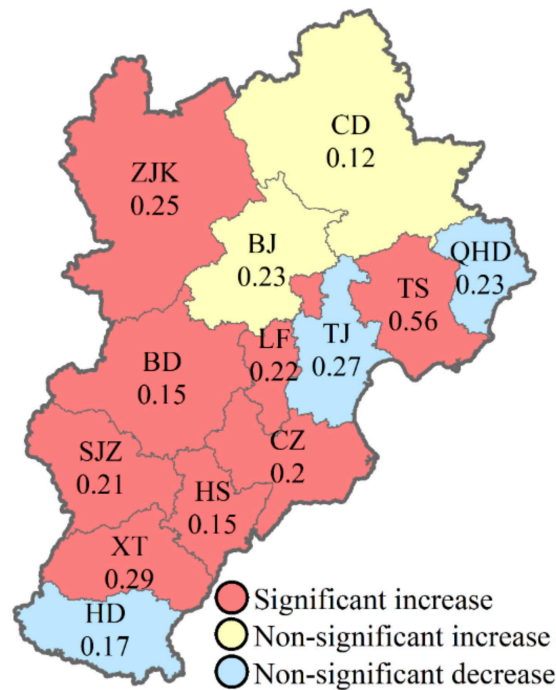


**Figure 4.** Trends in FP of cities in the BTH region, 2000–2020 (based on linear regression analysis). Values represent the rate of FP change (km/year).

### 3.2. Heat Exposure Risk Characteristics of Cities in the Beijing–Tianjin–Hebei Region

The results shown in Figure 5 indicate that the average annual population exposed to heat risk across the BTH region amounts to 32,965,265 people. Beijing has the greatest exposed population, with an annual average of 16,620,390 people; in cities with relatively high FP, such as Tianjin, Shijiazhuang and Tangshan, the annual average exposed populations are 5,734,637, 3,516,965 and 1,950,866 people, respectively; in Baoding, Handan and Qinhuangdao, the annual average exposed populations are 1,439,755, 1,406,141 and 876,725 people; the cities with only relatively small FP sizes, such as Cangzhou, Chengde, Hengshui, Langfang, Xingtai and Zhangjiakou, also have relatively small exposed populations of 567,910, 269,826, 440,763, 576,778, 836,982 and 643,950 people, respectively.

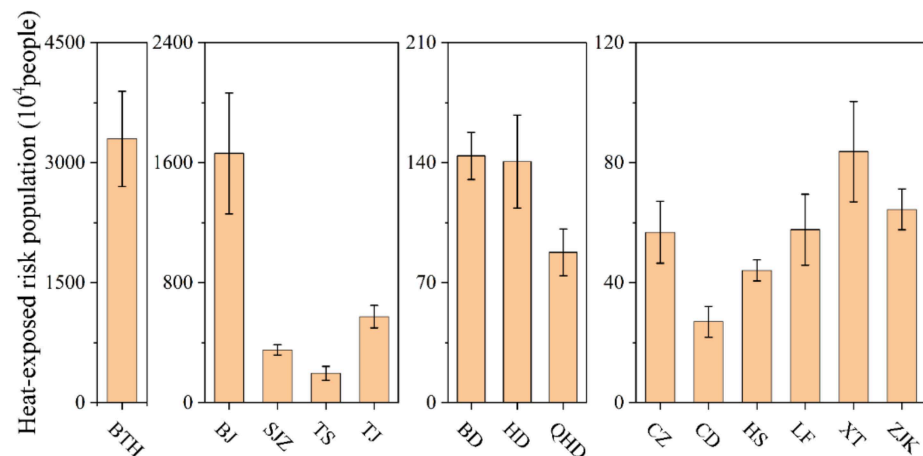


**Figure 5.** Statistical characteristics of the heat-exposed population in each city in the BTH region. The error bar represents the standard deviation of the exposed population in each city from 2000 to 2020.

The results of the linear analysis (Figure 6) show that, similar to the FP characteristics, there is a significant upward overall trend ( $p < 0.01$ ) in the exposed population across the BTH region. From 2000 to 2020, the total urban exposed population in the region increases from 24,350,510 to 41,138,167 people, with an average annual increase in 835,968 people based on linear regression. Except for Handan ( $-462$ , in people/year, the same below), all cities show increasing trends in the exposed population, with 11 cities showing significant increases ( $p < 0.01$ ). Among them, Beijing shows the highest growth rate of exposed population (645,878), followed by Tianjin (87,965), Tangshan (68,041), Shijiazhuang (51,006), Xingtai (20,012), Baoding (19,745), Langfang (16,807), Cangzhou (13,753), Zhangjiakou (9395), Qinhuangdao (8370), Chengde (5029) and Hengshui (4539).

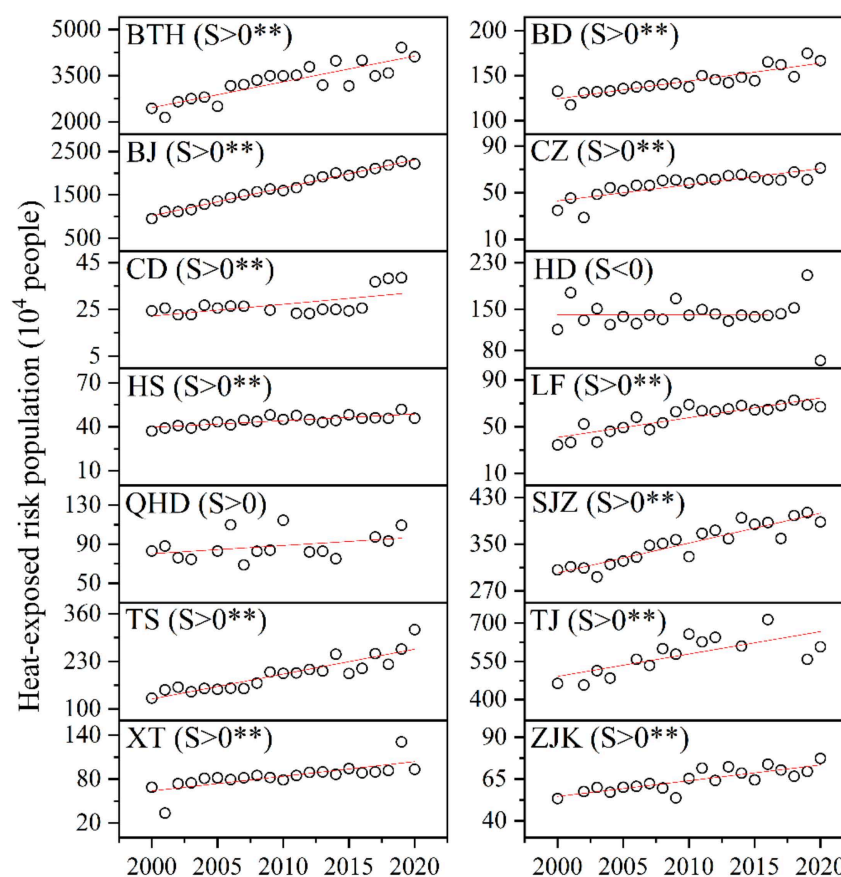


**Figure 6.** Trends of exposed population characteristics by city in the BTH region, 2000–2020 (based on linear regression analysis).  $S$  represents the slope, with  $S > 0$  showing an increasing trend and  $S < 0$  showing a decreasing trend; \*\*  $p < 0.01$ .

Notably, Figure 7 shows that the heat-exposed population in the study area is generally dominated by high-risk exposure, accounting for more than 65% of the total exposed population. Among the individual cities, Qinhuangdao has the highest proportion of the high-risk exposed population with an average of 70.47%, followed by Beijing (68.69%), Shijiazhuang (56.85%), Baoding (55.26%), Hengshui (50.90%), Tangshan (49.70%), Handan (47.74%), Tianjin (34.32%), Langfang (31.27%), Xingtai (28.89%) and Cangzhou (24.12%). In comparison, the proportion of the low-risk exposed population is highest in Chengde (25.67%), while the proportion of the medium-risk population is highest in Zhangjiakou (25.40%). In addition, the high-risk population in the BTH region shows an overall increasing trend during the study period, and fewer cities show decreasing trends, only Chengde and Zhangjiakou.

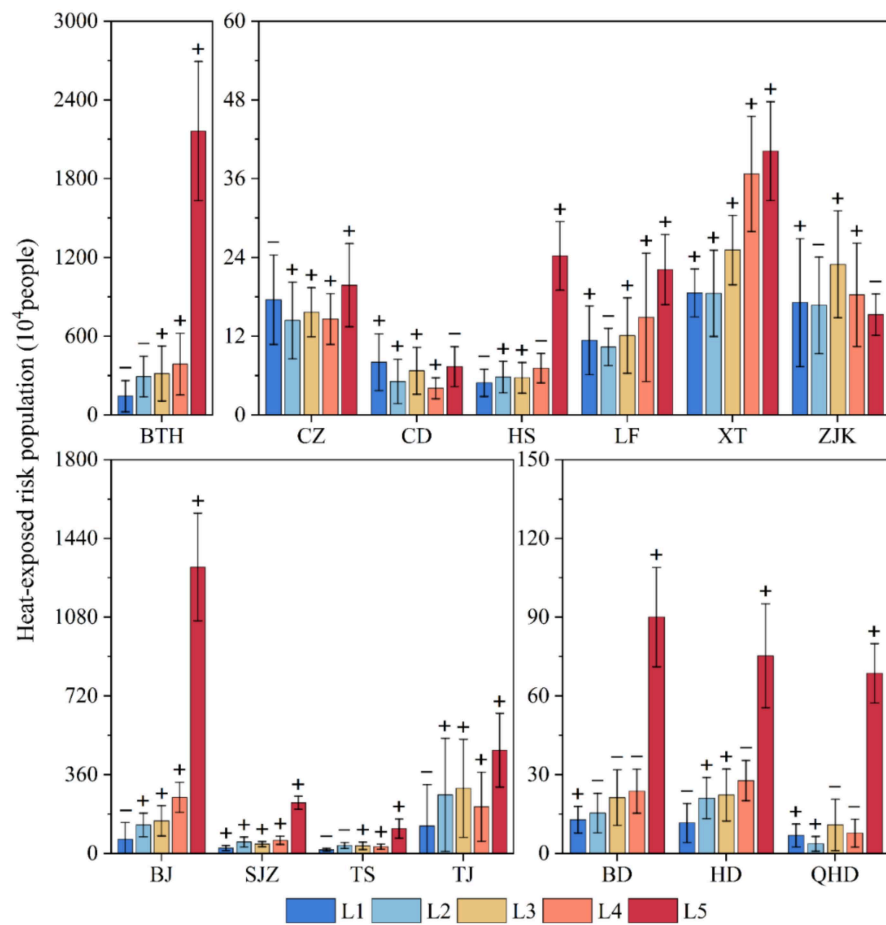


**Figure 7.** Statistical characteristics and trends of the heat-exposed population by level in cities of the BTH region (based on linear regression analysis). The error bar represents the standard deviation of the exposed population in each city. +/− represents the increasing/decreasing trend of the heat exposure risk population.

3.3. Characteristics of the Association between Heat Exposure Risk and Urbanization Elements

Figure 8 shows the fitted curves of the relationship between the heat exposure risk population and urbanization factors (BUA, PD, GDP) in the BTH region, and it can be seen that these curves all have high goodness of fit ( $R^2 > 0.60$ ), indicating that the urbanization factors all have strong explanatory power for the inter-city differences of heat exposure risk. With the increase in the level of urbanization, the heat-exposed population show significant non-linear (power function) growth trends ( $p < 0.01$ ). In contrast, PD had the best explanation for the variation of the heat-exposed population in the BTH region ( $R^2 = 0.97$ ) and its power index (6.89) is higher compared to the other two urbanization indicators, i.e., heat exposure risk will continue and accelerate with population clustering, which is particularly evident in cities with population densities above 1000 people/km<sup>2</sup>. In addition, the study finds a positive correlation between the population at risk and urbanization factors in all 12 cities in the study area except Handan, and 11 of them have significant relationships, further clarifying the general situation that the urbanization process increases the risk of heat exposure (Table 2).

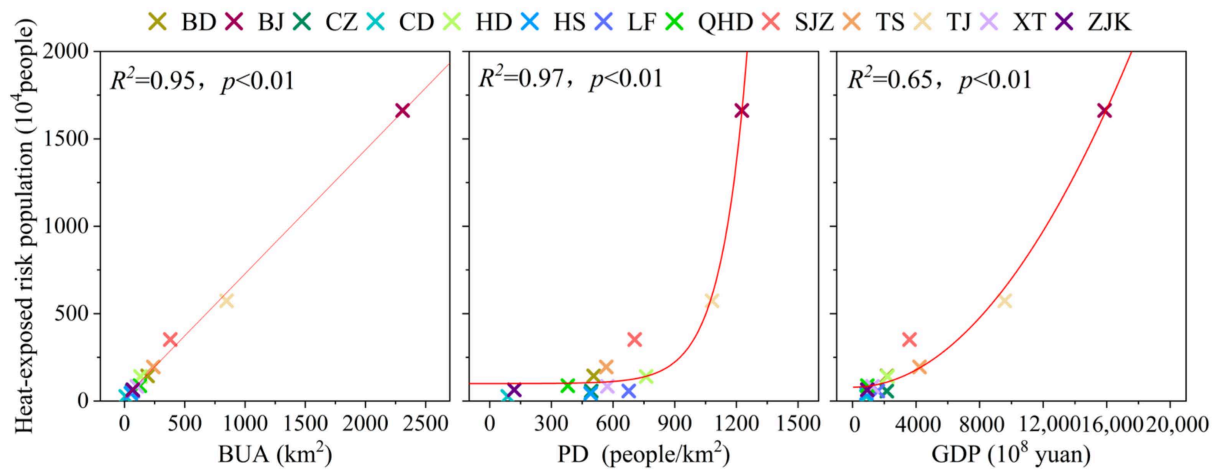


**Figure 8.** Best-fit curves between heat-exposed population and urbanization factors for cities in the BTH region. BUA: built-up area, PD: population density, GDP: gross domestic product.

**Table 2.** Correlation coefficients between urban heat-exposed population and urbanization factors in Beijing–Tianjin–Hebei region, 2000–2020.

	BUA	PD	GDP
BD	0.82 **	0.89 **	0.88 **
BJ	0.95 **	0.98 **	0.97 **
CZ	0.76 **	0.82 **	0.82 **
CD	0.95 **	0.59 **	0.51 **
HD	−0.22	−0.01	−0.01
HS	0.85 **	0.81 **	0.73 **
LF	0.91 **	0.87 **	0.82 **
QHD	0.38	0.17	0.37
SJZ	0.82 **	0.92 **	0.92 **
TS	0.89 **	0.91 **	0.88 **
TJ	0.56 **	0.67 **	0.83 **
XT	0.76 **	0.74 **	0.71 **
ZJK	0.83 **	0.83 **	0.76 **

\*\*  $p < 0.01$ . BUA: built-up area, PD: population density, GDP: gross domestic product.

The study also analyzes the association between the population within each heat exposure risk class and the urbanization process, and the results show significant power functions between the exposed population and urbanization factors in most of the risk levels (Figure 9). The power values of the association between the high-risk population and urbanization factors are all higher than those of the other risk levels, suggesting that as the region continues to urbanize, the population exposed to the high-risk areas grows significantly faster than the other risk levels.

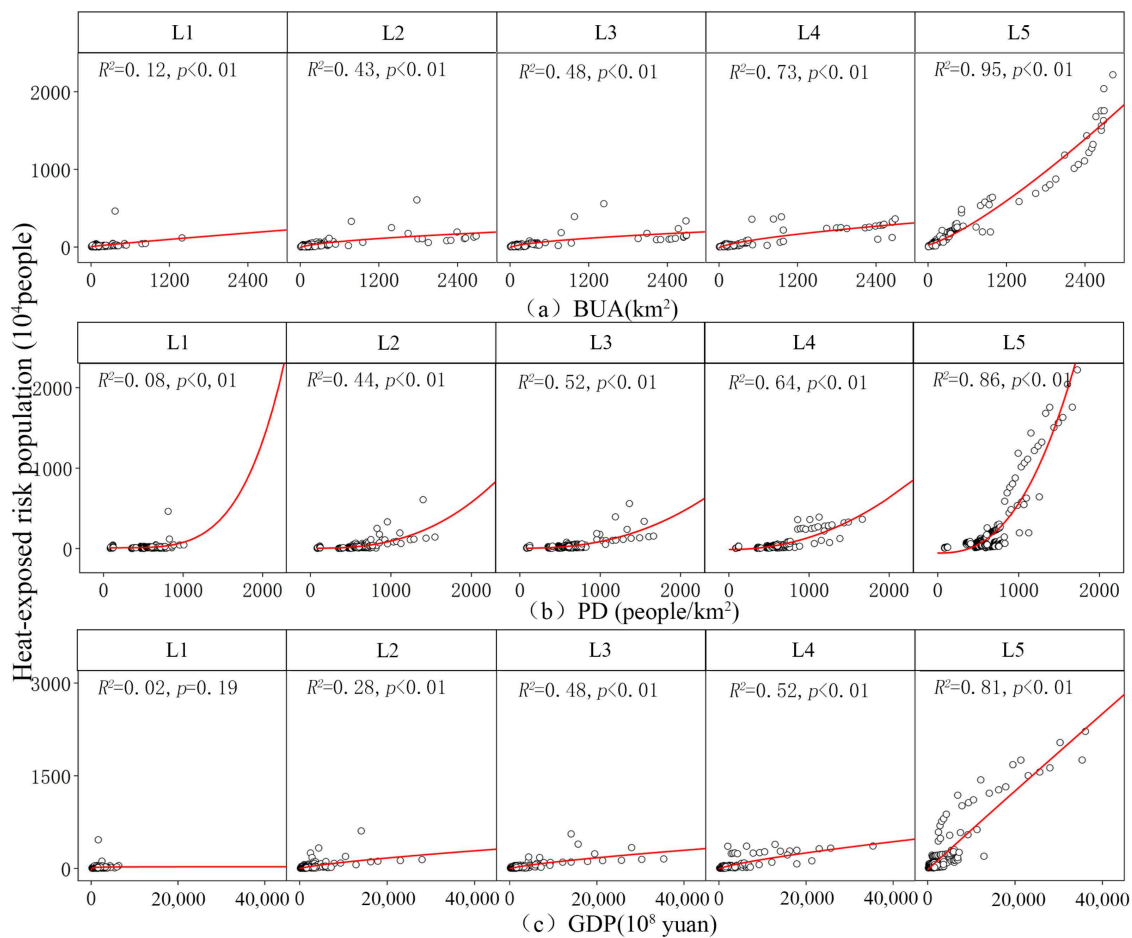


**Figure 9.** Best-fit curve of the relationship between heat exposure risk population by level and urbanization factors at all levels for cities in the BTH region from 2000 to 2020.

#### 4. Discussion

##### 4.1. Increased Risk of Heat Exposure in the BTH Region

This study systematically analyzes the heat exposure risk and its temporal trends in 13 cities in the BTH region based on FP. First, our study indicates the widespread presence of FP across cities in the BTH region (Figure 3), which is consistent with numerous previous studies [42,43]. During the study period, the average FP in each city ranges from 6.06 km (Chengde) to 32.51 km (Beijing). In addition, FP shows increasing trends in 10 cities except for Handan, Tianjin and Qinhuangdao (Figure 4), i.e., the extent of the influence of the UHI effect expanded during the study period, which would significantly enhance the risk of heat stress for massive populations in and around urban built-up areas. By overlaying the population raster data, it is found that there are large heat exposure risk population in the region, which is also consistent with the results of previous studies on heat exposure risk in the BTH region [44,45]. The average heat-exposed population in the region reaches 32,965,264 during the study period, which exceeds 33.25% of the total regional population and is higher than the proportion of the population in the urban built-up area (29.36%) (Figure 10), which confirms the spillover effect of the UHI effect and its impact on the population outside the urban built-up area [23,24]. In addition, the average exposed population varies from 269,826 (Chengde) to 16,620,390 (Beijing) across cities (Figure 5), with significant variations that could be attributed to the different urbanization levels of cities in the region (introduced in Section 4.2). Notably, the level of risk faced by the at-risk population in the region's cities is uneven. The majority of the population is exposed to high risk (Figure 7), which is higher than 65% in the region as a whole, and this would significantly increase the incidence of heat illnesses such as heat cramps, heat

exhaustion, heatstroke, with serious negative effects on the health of a large number of residents [9–11]. For this reason, it is necessary to take effective measures to reduce the extent of the UHI effects and their magnitude ( $\Delta T$ ) to mitigate its impact on human health and the human habitat.

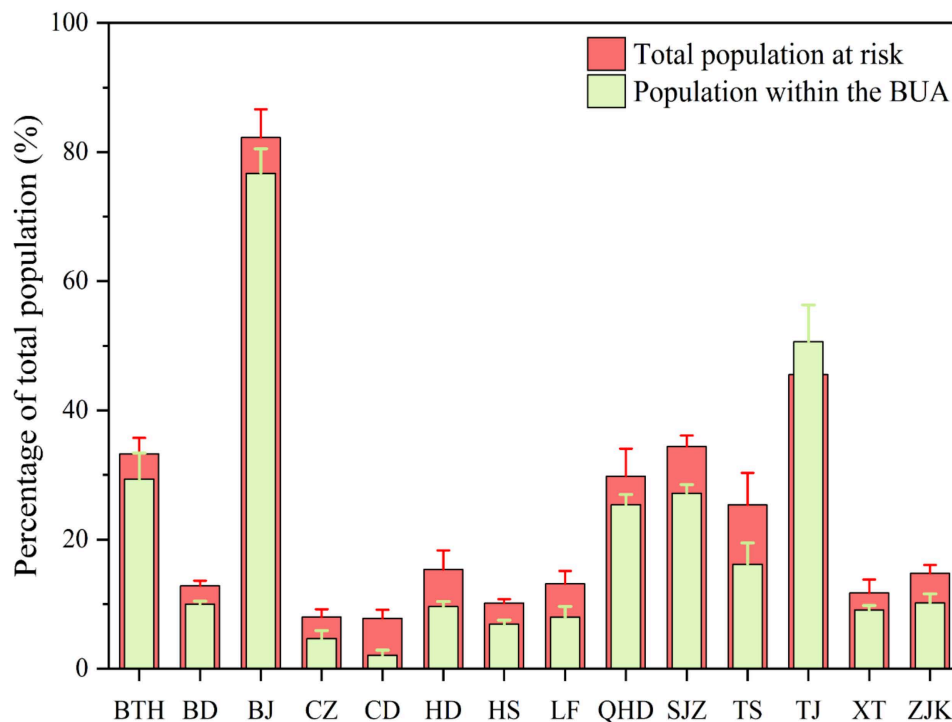


**Figure 10.** The proportion of heat exposure risk population to total population compared to the proportion of built-up area population to total population in the BTH region. The error bars represent the standard deviation of the at-risk population and the population within the built-up area from 2000 to 2020.

Unfortunately, we find general and significant increasing trends of heat exposure risk in the BTH region from 2000 to 2020 based on the results of the linear fit (Figure 6). Among the cities in the region, the heat exposure risk population shows increasing trends in all 12 cities except Handan, and 11 of them show significant increasing trends. In addition, the level of risk faced by each city is also increasing, especially the high risk, which shows increasing trends in all 11 cities except Chengde and Zhangjiakou. These results imply that in the coming decades, more urban residents will be exposed to high-heat environments and will face further increased heat exposure risk.

#### 4.2. Relationship between Heat Exposure Risk and Urbanization in the BTH Region

This study investigates the pairwise relationship between urbanization factors and heat exposure risk in the BTH region based on curve fitting and correlation analysis. The results show that cities with higher urbanization levels, such as Beijing, Tianjin, Shijiazhuang and Tangshan, tend to have populations at greater risk during the same period, and the level of heat exposure risk increases in most cities with increasing urbanization level, i.e., there is a significant positive correlation between urbanization level and urban heat exposure risk, which is consistent with related studies [44,46,47]. In the process of land urbanization, the rapid expansion of urban built-up areas has resulted in huge changes in land cover, and the natural ground surface is gradually replaced by artificial impervious surfaces, which in turn leads to a weakening of the cooling effect of vegetation, a decrease in surface albedo, a decrease in latent heat flux, and an increase in sensible heat flux, resulting in more residents being exposed to high temperatures and increasing the risk of

heat exposure [48–51]. In addition, we find an interesting phenomenon whereby, unlike PD and GDP, the trend of heat exposure risk growth gradually slows down with BUA expansion in the cities of the BTH region (Figure 8), which may be caused by the presence of lower impervious surface density and good landscape planning in the new urban areas, which can effectively regulate the LST and reduce the high thermal risk [52–54]. In terms of population urbanization, cities with high population densities may experience high levels of heat stress, as reported in previous studies, which often results from increased anthropogenic heat emissions due to high population concentrations [55,56]. In this study, it is found that urban heat exposure risk shows an accelerating trend with the elevation of PD. This may be due to a series of effects brought about by high population density, such as high-intensity energy consumption, high concentration of atmospheric pollution, etc., which play an enhancing role in the UHI effect, and this enhancing effect is not unidirectional, but one of circular feedback [26,42,57]. Moreover, there is a significant positive relationship between economic urbanization and the risk of heat exposure in the region. This is mainly due to both industrial clustering and industrial structures [58,59]. First, the rapid economic development in the BTH region, especially in cities such as Beijing and Tianjin, has led to the expansion and clustering of their industries, which have positive effects on amplifying heat stress in urban areas [60]. Furthermore, industrial structures also have an impact on the regional thermal environment. Previous studies have pointed out the enhancing effect of secondary industry on the UHI effect [58,60]. In the BTH region, there is the largest comprehensive industrial and manufacturing base in northern China, and cities like Tangshan and Shijiazhuang are typical industrial cities with a large number of traditional industries. While driving rapid economic development, these industries emit a large amount of greenhouse gases and industrial heat into the environment, resulting in the deterioration of the urban thermal environment and a high level of heat exposure risk. In contrast, the correlation between economic urbanization and thermal exposure risk is lower in cities such as Chengde and Qinhuangdao, probably since their leading industries include tourism, which has a weaker interaction with the thermal environment [61].

In addition, the study finds a high percentage of the population to be at high risk in the region, which is largely due to the specificity of urbanization. This specificity is mainly reflected in the fact that the closer one is to the core area, rather than the peri-urban area, the higher the intensity of human activity, economic activity and construction, and the resulting intensive anthropogenic heat emissions will lead to higher temperatures in the core area than in the peri-urban area [26]. Areas of population concentration overlap with areas at risk of heat exposure, exposing more people to high heat risk in urban centers.

#### 4.3. Implications and Limitations

This study provides a comprehensive assessment of the heat exposure risk in the BTH region based on the FP extracted from a single exponential decay model, and the results show that there is a large heat-exposed population in the cities within the region, which is generally higher than the population in built-up urban areas. This implies that the previous assessment method using urban built-up areas as the boundary is not sufficient for comprehensively assessing the heat exposure risk in the region. In addition, correlation analysis and optimal curve fitting confirm the driving effect of urbanization factors on heat exposure risk, especially high heat exposure risk, which provides a basis for appropriate measures to mitigate the negative effects on the population.

However, we also recognize some limitations of the present study. Firstly, it does not consider the differences in people themselves. Previous studies have shown that groups such as the disabled, the elderly, the less educated, and the poor have higher heat vulnerability and tend to have a higher risk of heat stress [62,63]. However, these data, especially those with high spatial resolution, are difficult to obtain. Secondly, the study only selected three representative urbanization indicators for pairwise analysis with heat exposure risk, which are relatively few and do not consider the combined effect of multiple factors, which may lead to an incomplete understanding of urban heat exposure

risk mechanisms. Finally, in addition to the heat stress risk, the interior of FP is often accompanied by other risks, such as high pollution risk. The atmosphere inside FP is heated to achieve upward movement, forming a low-pressure center, and the near-surface air in the surrounding areas converges to the interior of FP, which causes the sulfur oxides, nitrogen oxides, carbon oxides, and hydrocarbons generated from production and living activities in the region collect in the interior of FP, endangering human health. There is a need for further risk assessment based on FP [64]. In conclusion, the above uncertainties need to be considered and overcome in future studies.

## 5. Conclusions

This study extracts FP for 13 cities in the BTH region from 2000 to 2020 based on a single exponential decay model as a basis for identifying the spatial and temporal characteristics of heat exposure risk in the region and exploring their relationships with urbanization factors. The main findings are as follows:

(1) All cities in the BTH region are facing serious UHI problems, with the average FP of each city being in the order Beijing (32.51 km), Tianjin (17.84 km), Tangshan (17.53 km), Shijiazhuang (17.38 km), Qinhuangdao (13.65 km), Handan (13.31 km), Baoding (13.26 km), Langfang (9.82 km), Hengshui (9.42 km), Xingtai (9.03 km), Zhangjiakou (8.81 km), Cangzhou (7.99 km) and Chengde (6.05 km), all of which exceed the built-up area of the city. In addition, FPs show increasing trends in all cities except Tianjin, Qinhuangdao and Handan, with average annual growth rates ranging from 0.12 km/year (Chengde) to 0.56 km/year (Tangshan).

(2) The risks of heat exposure in the cities of the BTH region are prominent, with the average annual exposed population in the region reaching 32,965,265 people, with the cities in the following order: Beijing (16,620,390, in people, the same below), Tianjin (5,734,637), Shijiazhuang (3,516,965), Tangshan (1,950,866), Baoding (1,439,755), Handan (1,406,141), Qinhuangdao (876,725), Xingtai (836,982), Zhangjiakou (643,950), Langfang (576,778), Cangzhou (567,910), Hengshui (440,763) and Chengde (269,826), and are dominated by exposure to high-risk areas (more than 65% of the total). Meanwhile, all cities show increasing trends in the heat-exposed population at risk, except Handan, with average annual growth rates ranging from 4539 people/year (Hengshui) to 6,458,878 people/year (Beijing).

(3) There is a significant non-linear positive relationship between the urbanization process and the risk of heat exposure in the study area, indicating that as the economic development of cities, the increase in population density and the expansion of built-up areas increase, the size of the heat exposure risk in cities and the level of risk increase to varying degrees.

In general, as urbanization continues, heat exposure risks to urban populations in the BTH region will continue to be a problem, with serious negative impacts on the living environment and human health. Therefore, city managers and planners must pay more attention to the mitigation and management of urban heat exposure risks, and take more reasonable and effective measures to prevent further deterioration of urban heat risks.

**Author Contributions:** X.F.: Conceptualization, Methodology, Validation, Investigation, Data Curation, Writing—Original Draft, Visualization. L.Y.: Validation, Writing—Review and Editing, Supervision, Funding acquisition. S.S.: Software, Resources, Data Curation. All authors have read and agreed to the published version of the manuscript.

**Funding:** This study is funded by the National Natural Science Foundation of China (Grant No. 42171094) and the Natural Science Foundation of Shandong Province (Grant No. ZR2021MD095 and ZR2021QD093).

**Institutional Review Board Statement:** Not applicable.

**Informed Consent Statement:** Not applicable.

**Data Availability Statement:** Not applicable.

**Acknowledgments:** The authors are very grateful to the editors and anonymous reviewers for their valuable time and advice on this manuscript.

**Conflicts of Interest:** The authors declare that they have no known competing financial interest or personal relationships that could have appeared to influence the work reported in this paper.

## References

1. WORLD CITIES REPORT 2020: The Value of Sustainable Urbanization. Available online: <https://unhabitat.org/wcr/> (accessed on 1 December 2020).
2. Li, Y.; Zhou, D.; Yan, Z. Spatiotemporal variations in atmospheric urban heat island effects and their driving factors in 84 major Chinese cities. *Environ. Sci.* **2021**, *42*, 5037–5045. [[CrossRef](#)]
3. Liu, Z.; Wang, Y.; Peng, J. Remote sensing of impervious surface and its applications: A review. *Prog. Geogr.* **2010**, *29*, 1143–1152. [[CrossRef](#)]
4. Angel, S.; Parent, J.; Civco, D.L.; Blei, A.; Potere, D. The dimensions of global urban expansion: Estimates and projections for all countries, 2000–2050. *Prog. Plan.* **2011**, *75*, 53–107. [[CrossRef](#)]
5. Oke, T.R. City size and the urban heat island. *Atmos. Environ.* **1973**, *7*, 769–779. [[CrossRef](#)]
6. Aboelata, A. Vegetation in different street orientations of aspect ratio (H/W 1:1) to mitigate UHI and reduce buildings' energy in arid climate. *Build. Environ.* **2020**, *172*, 106712. [[CrossRef](#)]
7. He, B.; Wang, J.; Liu, H.; Ulpiani, G. Localized synergies between heat waves and urban heat islands: Implications on human thermal comfort and urban heat management. *Environ. Res.* **2021**, *193*, 110584. [[CrossRef](#)]
8. Jadraque, G.; Etxebarria, B.S.; Pacheco, T.R.; Muneer, T. Effect of Land Use/Cover Changes on Urban Cool Island Phenomenon in Seville, Spain. *Energies* **2020**, *13*, 3040. [[CrossRef](#)]
9. Peng, R.D.; Bobb, J.F.; Tebaldi, C.; McDaniel, L.; Bell, M.L.; Dominici, F. Toward a quantitative estimate of future heat wave mortality under global climate change. *Environ. Health Perspect.* **2011**, *119*, 701–706. [[CrossRef](#)]
10. Bobb, J.F.; Peng, R.D.; Bell, M.L.; Dominici, F. Heat-related mortality and adaptation to heat in the United States. *Environ. Health Perspect.* **2014**, *122*, 811–816. [[CrossRef](#)]
11. Ebi, K.L.; Capon, A.; Berry, P.; Broderick, C.; de Dear, R.; Havenith, G.; Honda, Y.; Kovats, R.S.; Ma, W.; Malik, A.; et al. Hot weather and heat extremes: Health risks. *Lancet* **2021**, *398*, 698–708. [[CrossRef](#)]
12. Quantitative Risk Assessment of the Effects of Climate Change on Selected Causes of Death, 2030s and 2050s. Available online: <https://apo.org.au/node/41763> (accessed on 1 December 2015).
13. Flouris, A.D.; Dinas, P.C.; Ioannou, L.G.; Nybo, L.; Havenith, G.; Kenny, G.P.; Kjellstrom, T. Workers' health and productivity under occupational heat strain: A systematic review and meta-analysis. *Lancet Planet. Health* **2018**, *2*, e521–e531. [[CrossRef](#)]
14. Working on a Warmer Planet: The Effect of Heat Stress on Productivity and Decent Work. Geneva: International Labour Organization. Available online: [http://www.ilo.org/global/publications/books/WCMS\\_711919/lang--en/index.htm](http://www.ilo.org/global/publications/books/WCMS_711919/lang--en/index.htm) (accessed on 1 July 2019).
15. Garcia, T.R.; Jarquín, E.; Wesseling, C.; Johnson, R.J.; Gonzalez, Q.M.; Weiss, I.; Glaser, J.; Jose, V.J.; Stockfelt, L.; Roncal, C.; et al. Heat stress, dehydration, and kidney function in sugarcane cutters in El Salvador—A cross-shift study of workers at risk of Mesoamerican nephropathy. *Environ. Res.* **2015**, *142*, 746–755. [[CrossRef](#)]
16. Ciuha, U.; Pogačar, T.; Bogataj, L.K.; Gliha, M.; Nybo, L.; Flouris, A.D.; Mekjavic, I.B. Interaction between Indoor Occupational Heat Stress and Environmental Temperature Elevations during Heat Waves. *Weather Clim. Soc.* **2019**, *11*, 755–762. [[CrossRef](#)]
17. Romero, L.P.; Hua, Q.; Dickinson, K. Urban vulnerability to temperature-related hazards: A meta-analysis and meta-knowledge approach. *Glob. Environ. Chang.* **2012**, *22*, 670–683. [[CrossRef](#)]
18. Hoehne, C.G.; Hondula, D.M.; Chester, M.V.; Eisenman, D.P.; Middel, A.; Fraser, A.M.; Watkins, L.; Gerster, K. Heat exposure during outdoor activities in the US varies significantly by city, demography, and activity. *Health Place* **2018**, *54*, 1–10. [[CrossRef](#)]
19. Hu, L.; Wilhelmi, O.V.; Uejio, C. Assessment of heat exposure in cities: Combining the dynamics of temperature and population. *Sci. Total. Environ.* **2019**, *655*, 1–12. [[CrossRef](#)]
20. Hsu, A.; Sheriff, G.; Chakraborty, T.; Manya, D. Disproportionate exposure to urban heat island intensity across major US cities. *Nat. Commun.* **2021**, *12*, 2721. [[CrossRef](#)]
21. Heaviside, C.; Macintyre, H.; Vardoulakis, S. The Urban Heat Island: Implications for Health in a Changing Environment. *Curr. Environ. Health Rep.* **2017**, *4*, 296–305. [[CrossRef](#)]
22. Li, H.; Zhou, Y.; Jia, G.; Zhao, K.; Dong, J. Quantifying the response of surface urban heat island to urbanization using the annual temperature cycle model. *Geosci. Front.* **2022**, *13*, 101141. [[CrossRef](#)]
23. Zhou, D.; Zhao, S.; Zhang, L.; Sun, G.; Liu, Y. The footprint of urban heat island effect in China. *Sci. Rep.* **2015**, *5*, 11160. [[CrossRef](#)]
24. Qiao, Z.; Wu, C.; Zhao, D.; Xu, X.; Yang, J.; Feng, L.; Sun, Z.; Liu, L. Determining the Boundary and Probability of Surface Urban Heat Island Footprint Based on a Logistic Model. *Remote Sens.* **2019**, *11*, 1368. [[CrossRef](#)]
25. Tao, F.; Hu, Y.; Tang, G.; Zhou, T. Long-Term Evolution of the SUHI Footprint and Urban Expansion Based on a Temperature Attenuation Curve in the Yangtze River Delta Urban Agglomeration. *Sustainability* **2021**, *13*, 8530. [[CrossRef](#)]
26. Yao, L.; Sun, S.; Song, C.; Li, J.; Xu, W.; Xu, Y. Understanding the spatiotemporal pattern of the urban heat island footprint in the context of urbanization, a case study in Beijing, China. *Appl. Geogr.* **2021**, *133*, 102496. [[CrossRef](#)]

27. National Bureau of Statistics. *China Statistical Yearbook*; China Statistics Press: Beijing, China, 2020.
28. Liu, Y.; Li, H.; Gao, P.; Zhong, C. Monitoring the Detailed Dynamics of Regional Thermal Environment in a Developing Urban Agglomeration. *Sensors* **2020**, *20*, 1197. [[CrossRef](#)]
29. Hou, L.; Yue, W.; Liu, X. Spatiotemporal patterns and drivers of summer heat island in Beijing-Tianjin-Hebei Urban Agglomeration, China. *IEEE J. Sel. Top. Appl. Earth Obs. Remote Sens.* **2021**, *14*, 7516–7527. [[CrossRef](#)]
30. Wan, Z. New refinements and validation of the MODIS Land-Surface Temperature/Emissivity products. *Remote Sens. Environ.* **2008**, *112*, 59–74. [[CrossRef](#)]
31. Lai, S.; Ruktanonchai, N.W.; Zhou, L.; Prosper, O.; Luo, W.; Floyd, J.R.; Wesolowski, A.; Santillana, M.; Zhang, C.; Du, X.; et al. Effect of non-pharmaceutical interventions to contain COVID-19 in China. *Nature* **2020**, *585*, 410–413. [[CrossRef](#)]
32. Lin, D.; Tan, Z.; Liu, K.; Liu, L.; Zhu, Y. Accuracy Comparison of Four Gridded Population Datasets in Guangdong Province, China. *Trop. Geogr.* **2020**, *40*, 346–356. [[CrossRef](#)]
33. National Bureau of Statistics. *China City Statistical Yearbook*; China Statistics Press: Beijing, China. Available online: <http://www.stats.gov.cn/english/Statisticaldata/AnnualData/> (accessed on 25 February 2022).
34. Rozenfeld, H.D.; Rybski, D.; Andrade, J.S.; Batty, M.; Stanley, H.E.; Makse, H.A. Laws of population growth. *Proc. Natl. Acad. Sci. USA* **2008**, *105*, 18702. [[CrossRef](#)]
35. Tan, M.; Li, X. Quantifying the effects of settlement size on urban heat islands in fairly uniform geographic areas. *Habitat Int.* **2015**, *49*, 100–106. [[CrossRef](#)]
36. Du, H.; Song, X.; Jiang, H.; Kan, Z.; Wang, Z.; Cai, Y. Research on the cooling island effects of water body: A case study of Shanghai, China. *Ecol. Indic.* **2016**, *67*, 31–38. [[CrossRef](#)]
37. Mathew, A.; Khandelwal, S.; Kaul, N. Spatial and temporal variations of urban heat island effect and the effect of percentage impervious surface area and elevation on land surface temperature: Study of Chandigarh city, India. *Sustain. Cities Soc.* **2016**, *26*, 264–277. [[CrossRef](#)]
38. Martin, V.J.; Sarricolea, P.; Moreno, G.M.C. On the definition of urban heat island intensity: The “rural” reference. *Front. Earth Sci.* **2015**, *3*. [[CrossRef](#)]
39. Lu, Y.; He, T.; Xu, X.; Qiao, Z. Investigation the Robustness of Standard Classification Methods for Defining Urban Heat Islands. *IEEE J. Sel. Top. Appl. Earth Obs. Remote Sens.* **2021**, *14*, 11386–11394. [[CrossRef](#)]
40. Peng, J.; Jia, J.; Liu, Y.; Li, H.; Wu, J. Seasonal contrast of the dominant factors for spatial distribution of land surface temperature in urban areas. *Remote Sens. Environ.* **2018**, *215*, 255–267. [[CrossRef](#)]
41. Wang, Y.; Yao, L.; Xu, Y.; Sun, S.; Li, T. Potential heterogeneity in the relationship between urbanization and air pollution, from the perspective of urban agglomeration. *J. Clean. Prod.* **2021**, *298*, 126822. [[CrossRef](#)]
42. Yang, Q.; Huang, X.; Tang, Q. The footprint of urban heat island effect in 302 Chinese cities: Temporal trends and associated factors. *Sci. Total Environ.* **2019**, *655*, 652–662. [[CrossRef](#)]
43. Hu, J.; Yang, Y.; Zhou, Y.; Zhang, T.; Ma, Z.; Meng, X. Spatial patterns and temporal variations of footprint and intensity of surface urban heat island in 141 China cities. *Sustain. Cities Soc.* **2022**, *77*, 103585. [[CrossRef](#)]
44. Luo, M.; Lau, N.C. Increasing heat stress in urban areas of eastern China: Acceleration by urbanization. *Geophys. Res. Lett.* **2018**, *45*, 13–060. [[CrossRef](#)]
45. Zhang, G.; Zeng, G.; Liang, X.-Z.; Huang, C. Increasing heat risk in China’s urban agglomerations. *Environ. Res. Lett.* **2021**, *16*, 064073. [[CrossRef](#)]
46. Wang, Q.; Zhang, Y.; Ban, J.; Zhu, H.; Xu, H.; Li, T. The relationship between population heat vulnerability and urbanization levels: A county-level modeling study across China. *Environ. Int.* **2021**, *156*, 106742. [[CrossRef](#)]
47. Luo, M.; Lau, N.C. Increasing Human-Perceived Heat Stress Risks Exacerbated by Urbanization in China: A Comparative Study Based on Multiple Metrics. *Earth’s Future* **2021**, *9*, e2020EF001848. [[CrossRef](#)]
48. Li, G.; Zhang, X.; Mirzaei, P.A.; Zhang, J.; Zhao, Z. Urban heat island effect of a typical valley city in China: Responds to the global warming and rapid urbanization. *Sustain. Cities Soc.* **2018**, *38*, 736–745. [[CrossRef](#)]
49. Zhou, D.; Zhao, S.; Liu, S.; Zhang, L.; Zhu, C. Surface urban heat island in China’s 32 major cities: Spatial patterns and drivers. *Remote Sens. Environ.* **2014**, *152*, 51–61. [[CrossRef](#)]
50. Yao, R.; Wang, L.; Huang, X.; Liu, Y.; Niu, Z.; Wang, S.; Wang, L. Long-term trends of surface and canopy layer urban heat island intensity in 272 cities in the mainland of China. *Sci. Total Environ.* **2021**, *772*, 145607. [[CrossRef](#)]
51. Zhang, Y.; Sun, L. Spatial-temporal impacts of urban land use land cover on land surface temperature: Case studies of two Canadian urban areas. *Int. J. Appl. Earth Obs. Geoinf.* **2019**, *75*, 171–181. [[CrossRef](#)]
52. Zhou, W.; Huang, G.; Cadenasso, M.L. Does spatial configuration matter? Understanding the effects of land cover pattern on land surface temperature in urban landscapes. *Landsc. Urban. Plan.* **2011**, *102*, 54–63. [[CrossRef](#)]
53. Rakoto, P.Y.; Deilami, K.; Hurley, J.; Amati, M.; Sun, Q. Revisiting the cooling effects of urban greening: Planning implications of vegetation types and spatial configuration. *Urban. For. Urban. Green.* **2021**, *64*, 127266. [[CrossRef](#)]
54. Li, J.; Song, C.; Cao, L.; Zhu, F.; Meng, X.; Wu, J. Impacts of landscape structure on surface urban heat islands: A case study of Shanghai, China. *Remote Sens. Environ.* **2011**, *115*, 3249–3263. [[CrossRef](#)]
55. Zander, K.K.; Cadag, J.R.; Escarcha, J.; Garnett, S.T. Perceived heat stress increases with population density in urban Philippines. *Environ. Res. Lett.* **2018**, *13*, 084009. [[CrossRef](#)]

56. Raj, S.; Paul, S.K.; Chakraborty, A.; Kuttippurath, J. Anthropogenic forcing exacerbating the urban heat islands in India. *J. Environ. Manag.* **2020**, *257*, 110006. [[CrossRef](#)]
57. Sun, R.; Lü, Y.; Yang, X.; Chen, L. Understanding the variability of urban heat islands from local background climate and urbanization. *J. Clean. Prod.* **2019**, *208*, 743–752. [[CrossRef](#)]
58. Su, H.; Han, G.; Li, L.; Qin, H. The impact of macro-scale urban form on land surface temperature: An empirical study based on climate zone, urban size and industrial structure in China. *Sustain. Cities Soc.* **2021**, *74*, 103217. [[CrossRef](#)]
59. Liu, X.; Ming, Y.; Liu, Y.; Yue, W.; Han, G. Influences of landform and urban form factors on urban heat island: Comparative case study between Chengdu and Chongqing. *Sci. Total Environ.* **2022**, *820*, 153395. [[CrossRef](#)]
60. Li, Y.; Sun, Y.; Li, J.; Gao, C. Socioeconomic drivers of urban heat island effect: Empirical evidence from major Chinese cities. *Sustain. Cities Soc.* **2020**, *63*, 102425. [[CrossRef](#)]
61. Sun, T.; Yang, L.; Sun, R.; Chen, L. Key factors shaping the interactions between environment and cities in megalopolis area of north China. *Ecol. Indic.* **2020**, *109*, 105771. [[CrossRef](#)]
62. Jalalzadeh, F.B.; Mahmood, R.; Hayes, M.; Rowe, C.; Abadi, A.M.; Shulski, M.; Medcalf, S.; Lookadoo, R.; Bell, J.E. Mapping Heat Vulnerability Index Based on Different Urbanization Levels in Nebraska, USA. *GeoHealth* **2021**, *5*, e2021GH000478. [[CrossRef](#)] [[PubMed](#)]
63. Aubrecht, C.; Özceylan, D. Identification of heat risk patterns in the U.S. National Capital Region by integrating heat stress and related vulnerability. *Environ. Int.* **2013**, *56*, 65–77. [[CrossRef](#)] [[PubMed](#)]
64. Jing, Z.; Liu, P.; Wang, T.; Song, H.; Lee, J.; Xu, T.; Xing, Y. Effects of Meteorological Factors and Anthropogenic Precursors on PM<sub>2.5</sub> Concentrations in Cities in China. *Sustainability* **2020**, *12*, 3550. [[CrossRef](#)]